ACS APPLIED MATERIALS & INTERFACES

Research Article

www.acsami.org

Free-Standing Optically Switchable Chiral Plasmonic Photonic Crystal Based on Self-Assembled Cellulose Nanorods and Gold Nanoparticles

Guang Chu,[†] Xuesi Wang,[‡] Hang Yin,[§] Ying Shi,[§] Haijing Jiang,[†] Tianrui Chen,[†] Jianxiong Gao,[†] Dan Qu,[†] Yan Xu,*[,†] and Dajun Ding[§]

[†]State Key Laboratory of Inorganic Synthesis and Preparative Chemistry, Jilin University, 2699 Qianjin Street, Changchun 130012, China

[‡]State Key Laboratory of Integrated Optoelectronics, College of Electronic Science and Engineering, Jilin University, 2699 Qianjin Street, Changchun 130012, China

[§]Institute of Atomic and Molecular Physics, Jilin University, 2699 Qianjin Street, Changchun 130012, China

Supporting Information

ABSTRACT: Photonic crystals incorporating with plasmonic nanoparticles have recently attracted considerable attention due to their novel optical properties and potential applications in future subwavelength optics, biosensing and data storage device. Here we demonstrate a free-standing chiral plasmonic film composed of entropy-driven self-*co*-assembly of gold nanoparticles (GNPs) and rod-like cellulose nanocrystals (CNCs). The CNCs−GNPs composite films not only preserve the photonic ordering of the CNCs matrix but also retain the plasmonic resonance of GNPs, leading to a distinct plasmon-induced chiroptical activity and a strong resonant plasmonic−photonic coupling that is confirmed by the stationary and ultrafast transient optical response. Switchable optical activity can be obtained by either varying the incidence angle of lights, or by taking advantage of the responsive feature of the CNCs matrix. Notably, an angle-dependent plasmon resonance in chiral nematic hybrid film has been observed for the first time, which differs drastically from that of the GNPs embed in three-dimensional photonic crystals, revealing a close relation with the structure of the host matrix. The current approach for fabricating device-scale, macroscopic chiral plasmonic materials from abundant CNCs with robust chiral nematic matrix may enable the mass production of functional optical metamaterials.

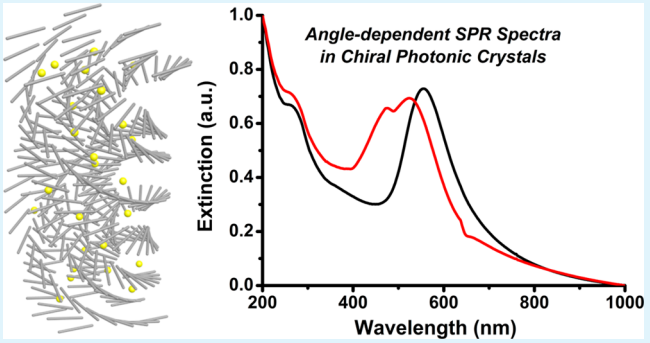

KEYWORDS: *photonic crystal, self-assembly, cellulose nanocrystals, plasmonic−photonic coupling, transient optical response, switchable optical activity*

INTRODUCTION

Photonic crystals are a class of materials with unique spatial periodicity in dielectric media, rendering them ability to manipulate light propagation when their lattice parameter is in the order of the wavelength of electromagnetic waves.[1,2] Self-assembly of nanoscale functional building blocks (e.g., quantum dots, noble metal nanoparticles and magnetic nanorods) into well-controlled photonic structure is gaining considerable attention due to its cost-efficient strategy compared to conventional top-down approach.[3−5] Incorporation of metal nanoparticles into photonic crystal is particularly interesting due to the anticipated functional integration may extend the potential applications to catalysis,[6,7] sensoring[8] and surface enhanced Raman spectroscopy.[9] As a unique class of photonic crystals, liquid crystal combines the flexibility and long-range orientational ordering together, and their optical properties can be tuned by external stimuli such as light,[10,11] irradiation[12] and electric field.[13] This may lead to smart materials with cheaper and more effective technology for large-scale production.

Recently, cellulose-based liquid crystalline nanomaterials have drawn increasing attention due to the intrinsic properties of cellulose including abundant availability, renewability, biodegradability, biocompatibility and excellent mechanical strength.[14−17] By controlled sulfuric acid-assisted hydrolysis, the extracted cellulose fibers can be transformed to cellulose nanocrystals (CNCs), which carry negative charges due to their surface sulfonate groups. CNCs are rigid twisted nanorods with excellent dispersibility in water.[18] When the concentration of the CNCs aqueous suspension is above a critical value, a phase separation occurs as Onsager previously predicted,[19] the

Received: June 25, 2015
Accepted: September 17, 2015
Published: September 17, 2015

DOI: 10.1021/acsami.5b05645
ACS Appl. Mater. Interfaces 2015, 7, 21797−21806

anisotropic CNCs may spontaneously assemble into a chiral nematic phase with orientational order that twists with a characteristic repeat distance termed as helical pitch.[20] Interestingly, the helical ordering of liquid crystalline CNCs can be preserved in solid chiral nematic films with brilliant and attractive colors as observed in some plants and crustaceans,[21,22] acting as a kind of one-dimensional chiral photonic crystal. This structure is also sensitive to the polarization of light, that is, selectively reflect the left-handed circularly polarized light, which can be considered as a natural polarization filter with a special photonic band gap (PBG).[23] Additionally, it is interesting to note that the chiral nematic ordering of CNCs can serve as a robust host matrix for a wide range of guest species including luminescent nanoparticles,[24−28] plasmonic nanorods[29−34] and polymeric microspheres,[35,36] generating new CNCs-based functional materials with coupled optical properties.

Research into the liquid crystalline CNCs-based materials has been mainly evolving around the chemical properties,[37] self-assembly characters,[16,17] templating for inorganic materials by confined mineralization[38,39] and the coassembly of guest−host interactions with functional nanoparticles.[29,32,35] However, to the best of our knowledge, the optical properties of the chiral nematic liquid crystalline CNCs-based material have not yet been explicitly exploited. Herein, we have designed a free-standing macrostructured solid composite film by using self-assembly strategy with plasmonic gold nanoparticles (GNPs) embedded into the chiral nematic scaffold of CNCs through the entropic driven process. Optical measurements such as polarized optical microscopy (POM), scanning electron microscopy (SEM) and focused ion beam microscopy (FIB) are utilized to study the anisotropic helicoidal structure of the host CNCs matrix and the distribution of the embedded guest GNPs. Meanwhile, a strong plasmonic−photonic coupling of the hybrid CNCs−GNPs films is demonstrated both in stationary and transient regimes for the first time, with the intrinsic photophysics of the hybrid system studied in detail. Furthermore, a switchable optical property of the composite film has been observed, reflecting the coupling effect between the PBG of chiral nematic CNCs matrix and the surface plasmon resonance (SPR) of GNPs. Because of the asymmetric chiral nematic ordering of the CNCs matrix, a plasmon-induced chiroptical activity has been found, indicating the interaction between GNPs and the chiral environment. Notably, an angle-dependent plasmonic extinction phenomenon is observed in the CNCs−GNPs composite film, which has never been found in other particle-embedded inverse opals.[40−44] On the basis of the results of the optical analysis, we hold that the angle-dependent SPR shifting of GNPs is closely associated with the chiral nematic structure of the CNCs−GNPs hybrid films. Thus, the chiral nematic CNCs−GNPs hybrid film of the current work may offer a new platform for developing device-scale ultrasensitive sensors based on these angle-sensitive plasmonic papers.

EXPERIMENTAL SECTION

Materials and Apparatus. All chemicals were obtained from commercial suppliers and used as received without further purification. Hydrogen tetrachloroaurate trihydrate ($HAuCl_4 \cdot 3H_2O$, 99.99%) was purchased from Acros Organics. Sodium citrate ($C_6H_7O_7Na$, 99%) was obtained from Beijing Chemical Works. Cotton pulp board was purchased from Hebei Paper Group of China.

Transmission electron microscopy (TEM) was conducted on a FEI Tecnai G2S-Twin with a field emission gun operating at 200 kV. Surface morphologies of the composite films were characterized by using a JEOL-6700F field emission scanning electron microscopy (SEM) instrument at an accelerating voltage of 3 kV Focused ion beam microscopy (FIB) was conducted on a Helios NanoLab 600i Dual-Beam system with a field emission gun operating at 15 kV to distinguish the distribution of GNPs in the hybrid composite. The texture image of the CNCs liquid crystal phase was conducted on a Leica DM400 M polarized optical microscopy (POM) instrument with images taken by polarizers in a perpendicular arrangement. A CCD camera (Leica DFC450C) was used for taking all the photographs of the samples. The steady-state adsorption UV−visible spectroscopy was carried out on a Shimazu UV-1800 spectrophotometer and the UV−vis-NIR spectroscopy was carried out on a Lambda 950 (PerkinElmer). Spectra were collected by mounting free-standing films so that the surfaces of the films were perpendicular or angled to the beam path. A homemade femtosecond laser system was used to measure the transient absorption spectra and the ultrafast dynamics of the sample. The details of the experimental setup have been described elsewhere.[45] The system produced fundamental laser using a Ti:sapphire pulse pumped oscillation and a regenerative amplifier (Spectral Physics) both operating at 1 kHz repetition rate. The output wavelength of the system was 800 nm where the full width at half-maximum (fwhm) was 90 fs and the output power was approximately 600 mW. Circular dichroism (CD) spectra were recorded on a BioLogic MOS-450 spectropolarimeter. Spectra were collected by mounting free-standing films with their surfaces perpendicular to the beam path. The electrophoretic mobility (ζ-potential) of CNCs and GNPs suspension was measured using a Malvern Zetasizer Nano-ZS90.

Synthesis, Assembly and Encapsulation of GNPs and CNCs. The GNPs and CNCs were synthesized according to the established procedures with the details provided in the Supporting Information.[27,46] Entropic driven, self-*co*-assembly of CNCs nanorods and GNPs was triggered by evaporating water from the mixed suspension with varying volume ratios of GNPs:CNCs (Supporting Information, Table S1). Typically, two aqueous suspensions of CNCs (3.2 wt %) and GNPs (2 nM) were mixed and stirred at room temperature for 30 min, leading to a homogeneous mixture. It was worth mentioning that the mixture was very stable for at least 1 month when it was sealed; no phase separation or particles aggregation occurred. Then, the mixture was poured into a polystyrene Petri dish (60 mm), followed by evaporation under ambient conditions for 4−6 days. Finally, free-standing chiral nematic films of CNCs and GNPs were obtained with a thickness of 0.5 mm, showing strong structured birefringence and plasmonic activity. This fabrication procedure can create large-area (cm^2-sized), chiral plasmonic composite film with high uniformity. For the purpose of comparison, the GNPs-free chiral nematic film of CNCs was prepared under the same conditions by using the aqueous CNCs only.

RESULTS AND DISCUSSION

Water-soluble GNPs with ζ-potential of −35.1 mV were synthesized via citrate reduction of $HAuCl_4$ and stabilized by citrate ligands.[46] As shown in Figure 1a, the mean core diameter of the GNPs is approximately 25 nm on the base of an analysis of the TEM micrograph. Figure 1b is a representative TEM image of the CNCs. High aspect ratio rod-like CNCs are observed with an average length and diameter of 250−300 and 15−20 nm, respectively. The ζ-potential of the CNCs nanorods is −65.4 mV. The ζ-potential can be used to measure the surface state and electrostatic repulsions, providing information on the stability of the colloidal system. When the value of the ζ-potential is smaller than ±15 mV, it can be used to indicate the onset of particle agglomeration. However, values greater than ±30 mV generally imply that there is sufficient mutual repulsion to induce the colloidal stability.[47] On the basis of the above analysis, both the suspensions of CNCs and GNPs

DOI: 10.1021/acsami.5b05645
ACS Appl. Mater. Interfaces 2015, 7, 21797−21806

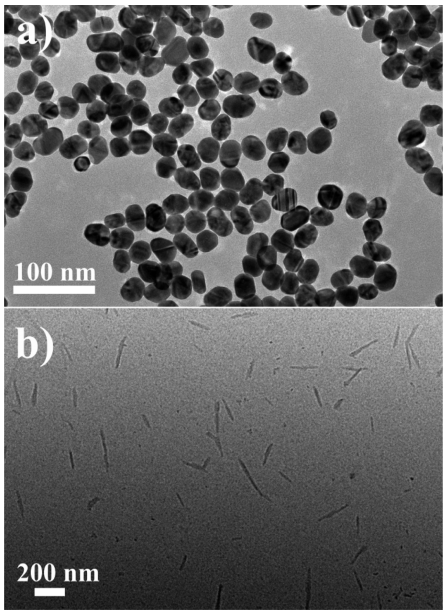

Figure 1. Representative TEM images of (a) GNPs and (b) CNCs nanorods.

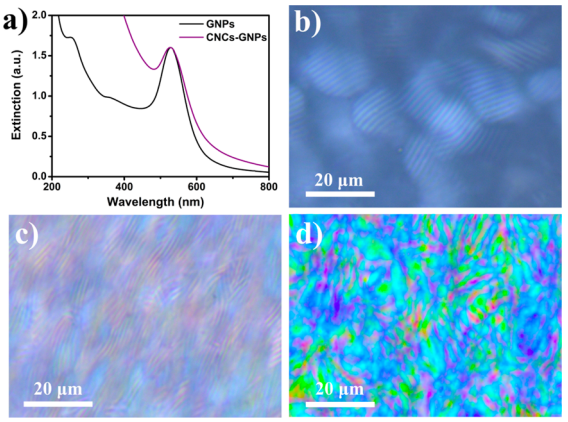

Figure 2. (a) Steady-state UV−visible spectra of the GNPs suspension and CNCs/GNPs mixed suspension, respectively. (b) POM image of the CNCs/GNPs mixture during evaporation, showing fingerprint textures. (c) POM image of the liquid crystalline CNCs/GNPs mixture with the evaporation continued, exhibiting a compressibility effect in helical pitch. (d) POM image of the dried CNCs/GNPs composite with characteristic marble-like texture, indicating the reservation of the chiral nematic architecture. All the images were taken with the polarizers in a crossed arrangement.

are homogeneously dispersed with strong colloidal stability. It should be noted that the type of surface charge of guest nanoparticles affects the self-assembly property of the CNCs nanorods. That is, the chiral nematic order of the CNCs liquid crystal can be perfectly preserved in solid film with negatively charged nanoparticles. In contrast, the addition of positively charged nanoparticles can lead to gelation of the CNCs nanorods due to the ionic interaction as well as the formation of particle flocculation.[30,36] As a result, the chiral nematic ordering of the CNCs composite film can be disrupted.

The chiral nematic CNCs−GNPs composite film, designated as CNCG film, was prepared by evaporation-induced self-*co*-assembly of CNCs nanorods and spherical GNPs. A series of samples have been obtained by varying the volume fractions of GNPs used relative to CNCs nanorods, yielded films with optically tunable PBG for CNCs matrix and chiroptical activities for GNPs (Table S1, Supporting Information). Because the chiral nematic ordering of the composite film is determined by the liquid crystalline CNCs, it is necessary to test whether the mixed CNCs−GNPs suspension could form a chiral nematic phase during the evaporation process. The optical properties of a 50:50 CNCs−GNPs suspension and a pure GNPs suspension were initially tested by the steady-state UV−visible spectra. As shown in Figure 2a, a typical SPR band centered at 528 nm is found in the extinction spectra of GNPs and the 50:50 CNCs−GNPs suspension. The SPR wavelength of the mixed suspension is the same as the pure GNPs, implying that no GNPs aggregation occurs.[46] The broader SPR bandwidth of the mixed suspension may be due to the scattering of the CNCs nanorods during absorption of light. After the optical measurement, the mixed suspension is introduced into a liquid crystal cell and drop-casted at room temperature with the evaporation process tracked by the POM technique. When the concentration of the mixed suspension is too low for the liquid crystalline phase to form, the droplets appear black when viewed under crossed polarizers (Figure S1). As the evaporation proceeds, a fingerprint texture begins to show, suggesting the formation of chiral nematic phase of CNCs coassembly with the GNPs (Figure 2b).[48] The helical pitch of the chiral nematic structure is evaluated by measuring the spacing between two adjacent lines of the fingerprint texture, showing an initial value of 2.4 μm (Figure 2b). As the evaporation continues, the helical pitch decreases to 1.6 μm, indicating a compression of the helical ordering likely due to water evaporation (Figure 2c). When the water in the mixture is fully evaporated, a marble-like texture is observed with a strong bright birefringent pattern, demonstrating the existence of chiral nematic ordering in the CNCG composite film (Figure 2d).

The chiral nematic structure of the self-assembled host CNCs nanorods as well as the distribution of guest GNPs were directly characterized by SEM, POM and FIB imaging of the CNCG composite film. The high magnification SEM image of a CNCG composite shows typical chiral nematic ordering at cross-sectional view (Figure 3a). At the fracture surfaces, an extensive periodic structure of the aligned CNCs nanorods with counterclockwise helical morphology has been observed. This long-range twisted organization of the CNCs nanorods confirms the one-dimensional photonic crystal structure that is responsible for the selective reflection of circularly polarized light.[22,38] Figure 3b is a low magnification SEM image of the side view of the cracked composite film. A stacking layered appearance was obtained, which derived from the helical pitch of the chiral nematic structure. The repeating distance is measured in the order of several hundred nanometers, which is in agreement with the estimated value based on the visible light spectra. The helicoidal architecture of the composite film is further confirmed by POM imaging analysis, showing well-pronounced fingerprint diffraction textures with strong birefringence and domains with different orientations, characteristic of the chiral nematic ordering (Figure 3c). The helical pitch is measured to be around 1.3 μm based on POM, similar to the value obtained from SEM imaging (Figure 3b, with measured pitch of 1.1 μm). In the CNCG composite film, it is very fascinating to know the relationship between CNCs nanorods and GNPs. As shown in Figure 3d, the location of GNPs is clearly visible on the high magnification FIB imaging

DOI: 10.1021/acsami.5b05645
ACS Appl. Mater. Interfaces 2015, 7, 21797−21806

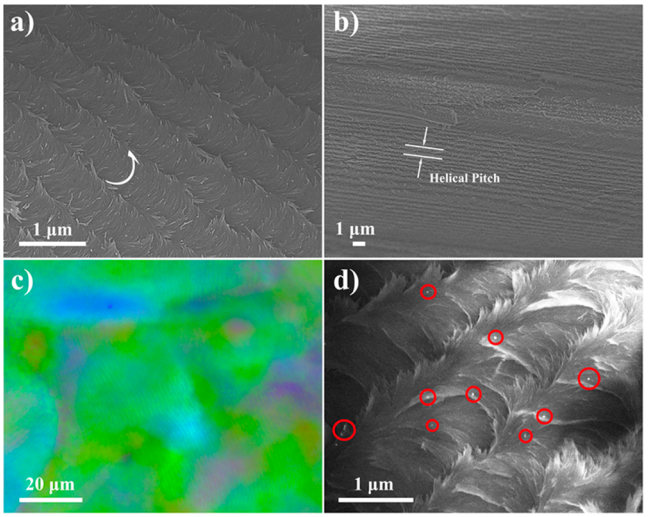

Figure 3. (a) Magnified SEM image of the CNCG-2g composite with cross-sectional view, showing a large area of counter-clockwise twisted arrangement of the rod-like CNCs. The arrow indicates a 180° counter-clockwise rotation of the director. (b) Side view of the cracked CNCG-2g film exhibits the stacked layers which derived from the helical pitch of the chiral nematic phase. (c) High-magnification POM image of the CNCG-2g film with a mass of periodic fingerprint textures. (d) Magnified FIB image of CNCG-2g showing the distribution of GNPs in CNCs host matrix. GNPs are circled by the red rings.

analysis due to its evidently different electric conductivity from that of CNCs. A cross section view of the CNCG composite film sliced longitudinally using ion beam shows that GNPs stay apart, and distribute randomly in the layered CNCs host matrix. Note that the interparticle spacing between two adjacent GNPs is much larger than the size of particle, the embedded GNPs in resulting films do not have any physical contacts with each other, no particle agglomeration occurs. The monodispersity of GNPs in the CNCs host matrix is very important as dipole coupling in the patterned nanocomposites causes the collective SPR wavelength peak to shift depending on the distance between nanoparticles.[49] On the basis of the FIB analysis of GNPs, due to the low GNPs concentration in the resulting hybrid films, the electromagnetic interactions between adjacent GNPs can be negligible and the effects of near- or far-field interaction between GNPs on their optical response can also be neglected.[50] Thus, the only contribution to the extinction of light then derived from nonradiative losses in the GNPs, that is, absorption. On the other hand, the distribution uniformity of GNPs inside the composite is depending on the interparticle Coulomb repulsions between negatively charged guest–host building blocks (GNPs-to-GNPs and GNPs-to-CNCs) through the entropic driven assembling process.[30]

The photonic property of the CNCG composite film can also be assessed through the UV–visible spectrum. Figure 4 are the steady-state extinction spectra of the CNCG composite films with different GNPs:CNCs ratios. All the composite films have similar thickness and exhibit strong iridescence. The PBG of the chiral nematic NPs-free CNCs film (CNCG-1a) is centered at 275 nm. The composite films of varying GNPs:CNCs ratios show two distinct peaks centered at 275 and 544 nm, respectively. The former is ascribable to the PBG of the CNCs matrix and the latter is associated with the collective SPR band of GNPs. It should be noted that the collective SPR

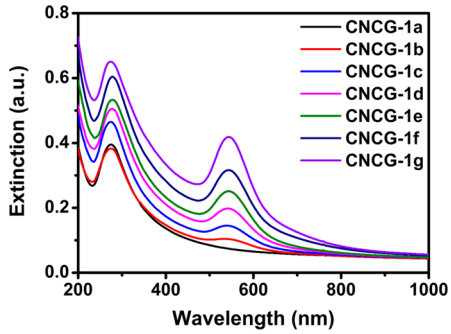

Figure 4. Steady-state UV–visible spectra of CNCG composite films with varying GNPs contents, showing an increase in SPR intensity for GNPs and invariant PBG positions.

peaks of GNPs in the CNCs matrix slightly shift to longer wavelengths compared to the isotropic GNPs suspension (Figure 2a), which is likely attributed to the increasing of medium refractive index from that of water (n = 1.33) to CNCs (n = 1.56).[29] During the entire range of GNPs loading, the intensity of the collective SPR band increases with the loading amounts of GNPs, but the PBG of CNCs host matrix stay stationary, implying that the interparticle electrostatic repulsions between CNCs have not been much changed with the addition of GNPs. This may be due to the conformability between negatively charged CNCs and GNPs and the low ionic strength in GNPs suspension.

It is known that the PBG of a chiral nematic CNCs matrix can be tuned by altering the electrostatic repulsions between CNCs nanorods, e.g., ultrasonication[51] and adding electrolytes[52] to the CNCs suspension prior to film casting. Therefore, a relative query naturally takes for granted as whether we can couple the GNPs collective SPR band with PBG of the CNCs matrix. Figure 5a shows the steady-state extinction spectra of the CNCG samples. Three series of the CNCG composites are prepared by loading the same amount of GNPs into the CNCs matrix with varying PBG ranging from ultraviolet to near-infrared, designated as CNCG-1g, CNCG-2g and CNCG-3g, respectively. The POM images of the three composite films show typical marble-like texture, confirming the chiral nematic ordering (Figure S2). CNCG-1g and CNCG-3g exhibit a distinct collective SPR peak centered at 544 nm with similar intensity. The central positions of the PBG for CNCG-1g (centered at 275 nm) and CNCG-3g (centered in the near-infrared spectrum range, Figure S3) are away from the collective SPR bands of GNPs, hence, no coupling or surface electromagnetic energy transfer is likely to occur between them. In the case of CNCG-2g, the situation is different as the PBG of the CNCs host matrix overlaps with the collective SPR band of GNPs, generating a coupled single peak centered at 556 nm with extraordinary high extinction intensity. The results demonstrate that the resonant coupling of a localized surface plasmon mode and a cavity mode in photonic CNCs matrix can strongly tailor the stationary optical response of GNPs. Prior works manifest that the surface electromagnetic waves in PBG and surface plasmons in nanostructured metallic particles are both nonradiative mode, and they can couple directly to each other in neighboring media, generating a modulated SPR-PBG optical property.[53] However, the static UV–vis spectra can only indicate the existence of a coupling between the photonic resonant modes of CNCs matrix and the plasmonic modes of GNPs, we still cannot extract the intrinsic nature of the hybrid

DOI: 10.1021/acsami.5b05645
ACS Appl. Mater. Interfaces 2015, 7, 21797–21806

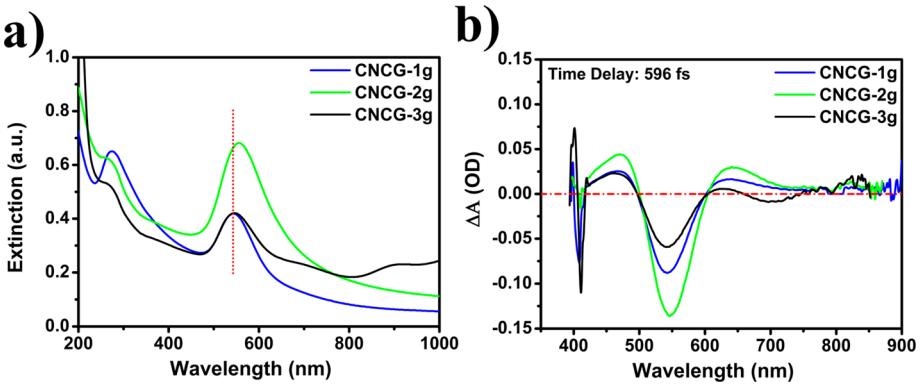

Figure 5. (a) Steady-state UV−visible spectra of the CNCG sample, exhibiting the coupling between SPR band of GNPs and tunable PBG for CNCs host matrix. (b) Transient adsorption spectra for the CNCG samples at their maximum, that is, just after optical pumping.

plasmonic−photonic coupling. In the strong coupling regime, the interactions become so strong that the new hybrid plasmonic−photonic states are formed by rapid photon exchange.[54] The great advantage of the transient absorption spectroscopy technique is its capability to measure small absorbance changes. It can be used to distinguish the difference in the transient absorption spectra of the ground state and the generation of the excited states, and therefore robust information on the existence of the plasmonic−photonic hybrid states can be provided.

The ultrafast transient optical response of the CNCG films is measured by 150 fs pump−probe laser spectroscopy with the excitation pump pulse wavelength at 400 nm. It should be noted that all of the CNCG films have no absorption peak at 400 nm (Figure 5a); only GNPs can be excited, which corresponds to the 5d→6sp interband transition of gold electrons. The resulting transient absorption spectra for CNCG films are displayed in Figure 5b. The transient spectra of the CNCG films show two positive peaks at around 470 and 640 nm, respectively, and a strong negative peak at around 545 nm, which differ from the corresponding steady-state UV−vis results (Figure 5a). The transient adsorption data for CNCG samples reveal a symmetric spectral profile at the SPR band, that is, with one negative transient peak and two positive wings. This phenomenon can be attributed to the "plasmon bleaching" behavior that is common for noble metal nanoparticles.[55] To study the resonant coupling effect between SPR and PBG, we chose the sample of CNCG-1g and CNCG-3g as the references due to their PBG are positioned far away from the SPR of GNPs. For the sample of CNCG-2g (whose PBG overlaps with the SPR of GNPs), it can be noticed that the coupling with the PBG not only results in the sharpening of the spectral profile of the photoinduced absorbance modulation but also leads to its large enhancement of the intensity of the negative transient peak. The sharpening derived from the restriction of the absorbance to the PBG of CNCs host matrix. And the enhancement is related to the trapping of both the pump and probe field within the photonic crystal cavity.[54] Moreover, it also should be noticed that an ultrafast SPR spectral shift is observed in the transient adsorption of CNCG samples. For the sample of CNCG-2g, the distinct negative transient peak is located at 546 nm. However, for the sample of CNCG-1g and CNCG-3g, this transient peak is blue-shifted to 542 nm. This phenomenon implies that the coupling of SPR mode and PBG can modulate the transient adsorption of GNPs, leading to a transient peak shifting. On the basis of the transient optical analysis above, we can confirm a strong plasmonic−photonic coupling occurs within the sample of CNCG-2g. In addition, these results also demonstrate that the resonant coupling of plasmonic−photonic modes not only enables us to tailor the stationary optical response of GNPs but also can lead to the large enhancement, spectral shaping and shifting of their transient optical response.

Further insights into the PBG-SPR coupled optical activity of the CNCG samples are obtained by analyzing their CD spectra. Figure 6 shows the variation in CD signals of the corresponding

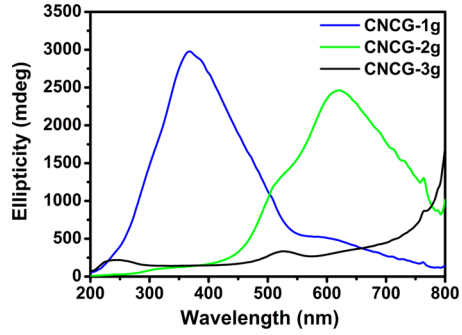

Figure 6. CD spectra of the CNCG films showing the tunability in left-handed organization and intense plasmon induced chiroptical activity of the embedded GNPs.

CNCG composite films. Because of the presence of macroscopic anisotropy in oriented films, the artifacts originating from linear dichroism/linear birefringence should be disregarded (Supporting Information, Figures S4 and S5).[56] All the samples exhibited strong positive Cotton bands through the entire spectra range that can be recognized as the combined peak of the corresponding left-handed CNCs matrix and GNPs plasmonic mode. The CD spectrum of CNCG-1g reveals the characteristic CD peak of chiral photonic crystal centered at 370 nm associated with the CD depression resonance band of the SPR mode for GNPs (at 536 nm). The spectrum of CNCG-2g shows a strong split in the CD band with a shoulder at 527 nm and a peak at 616 nm, which could be assigned to the SPR induced CD signal and scattering of the chiral CNCs matrix, respectively. The spectrum of CNCG-3g shows two distinct CD bands with a positive Cotton effect centered at 238 nm (corresponding to the molecular chirality of D-glucose units) and 527 nm (corresponding to SPR induced CD signal of GNPs), respectively. Comparing with the GNPs-free chiral

DOI: 10.1021/acsami.5b05645
ACS Appl. Mater. Interfaces 2015, 7, 21797−21806

nematic CNCs films (Figure S6), all three samples with different positioned PBGs show evident chiroptical activities at the SPR wavelength for GNPs, suggesting that the SPR induced CD mechanism arising from the interaction between GNPs and the chiral environment of CNCs host matrix is significant.[57] Additionally, it is worth mentioning that the intensities of the CD signals at SPR wavelength for these films are different, implying the varying degree of the coupling effects between the chiral photonic CNCs matrix and GNPs.

In a chiral nematic structure, the peak wavelength (λ) reflected by layered photonic ordering for incident light, causing the PBG, which can be expressed as

$$\lambda = n_{\text{eff}} \cdot P \cdot \sin\theta$$

where n_{eff} is the average refractive index of the chiral nematic material, P is the helical pitch and θ represents the angle between incident light and the surface normal of the film.[58] For CNCG materials, the average refractive index is constant due to the primary substrate composed by CNCs nanorods (n_{eff} = 1.56). Therefore, the λ can be tuned by changing either the helical pitch or the angle of incident light. We have demonstrated that ultrasonication is able to vary the λ of the CNCG composite films across a wide spectra range by altering the helical pitch, exhibiting a coupled SPR-PBG optical property. There comes an intriguing question: when the CNCG composite is fixed for sure, whether can we effectively manipulate the relative shifts between SPR band of GNPs and PBG diffraction peak of CNCs matrix?

Owing to the hydrophilicity of the CNCs matrix, the CNCG films swell rapidly upon immersion in polar solvents (e.g., water, ethanol and their mixtures of varying ratios), resulting in a red shift of the PBG as the helical pitch lengthens.[59−61] Taking CNCG-2g for example, it provides an ideal basis for controlling the separation of coupled SPR-PBG optical property. Figure 7 shows the UV−visible spectra of CNCG-2g before and after the immersion in water−ethanol mixture, respectively. Before immersion, the composite film exhibits a characteristic SPR-PBG band centered at 556 nm. Immersion of the composite film in a water−ethanol mixture (50:50 V/V %, n = 1.346) reduces the average refractive index of the composite film, and a consequential increase in the helical pitch attributed to the swelling. As a result, the UV−visible spectrum shows a separation of the coupled SPR-PBG peak, namely, the PBG red-shifts to 724 nm with an increase in the helical pitch, and the SPR mode of GNPs blue-shifts to 535 nm due to its sensibility to the surrounding medium. Such a shift is reversible that the UV−visible spectrum of the film resumes its original form upon drying (Figure S7). This change is both reversible and easily detectable by the UV−visible spectroscopy, which may enable the development of new plasmonic-based humidity sensors.

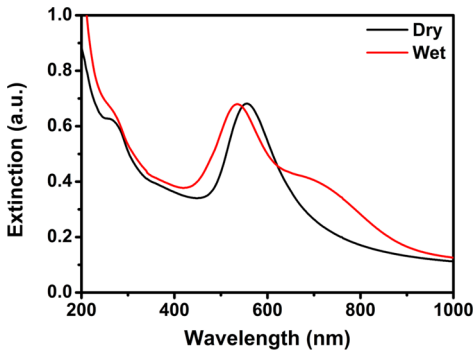

Figure 7. Steady-state UV−visible spectra of the sample CNCG-2g before (black line) and after (red line) soaked in EtOH/H_2O mixture. The refractive index of the mixture is 1.346.

More interestingly, the versatility of this switchable plasmonic optical property of the CNCG film can be further tuned by varying the incidence angle of light, θ. We systemically investigated the evolution of the steady-state UV−visible spectra at different incidence angles for the CNCG composite films, and changed the angle of the incident electromagnetic wave in small decrements ($\Delta\theta$ = 5°) from the normal (θ = 90°) to the grazing incidence angle value θ fixed at 30°. CNCG-1g with the PBG of CNCs matrix away from the collective SPR band of GNPs was studied first. Figure 8a is the angle resolved extinction spectra of CNCG-1g. Decreasing the angle of incident light from 90° to 30° causes a distinct blue shift of the PBG peak wavelength of the chiral nematic CNCs matrix. The total angle-dependent band shift in wavenumber ($\Delta\lambda_{\text{PBG}}$) is about 32 nm. To establish a quantitative relationship, the peak position of PBG of the CNC matrix was plotted against the sine of angle of incidence (sin θ), showing a linear relationship as shown in Figure 8b. The monotonic shifts observe in PBG peak wavelength, which can be attributed to the changes in diffraction related to incidence angles based on the above-mentioned diffraction equation. It is interesting to note that the collective SPR band of the CNCG film shows an angle-dependent plasmonic shifting, and the bandwidth of the collective SPR band narrows with the decrease of incidence angle. The collective SPR band is blue-shifted with the decrease of incidence angle, exhibiting a nonlinear relationship between them (Figure 7c). Initially, the collective SPR peak wavelength is centered at 544 nm with the incident wave at normal incidence (θ = 90°). It changes slightly to smaller values when the incidence angle decreases. The total blue shift value for the collective SPR band is $\Delta\lambda_{\text{SPR}}$ = 6 nm (from λ_{SPR} = 544 nm to λ_{SPR} = 538 nm). It is worth mentioning that the angle-dependent shift ($\Delta\lambda$) of PBG of the CNCs matrix is larger than that of the collective SPR band of GNPs, implying that they had different angle-dependence behavior. These optical measurements demonstrate that the CNCG composite film possessed a combination of an angle-dependent extinction band both in the PBG of the CNCs matrix and the collective SPR band of the embedded GNPs.

Because of the differences in angle-dependent shifting values between the PBG of the CNCs matrix and the collective SPR band of GNPs, an interesting hypothesis comes to our mind that whether the coupled SPR-PBG optical property can be reseparated by varying the incidence angle? Figure 8d shows the angle resolved extinction spectra of CNCG-3g, in which the PBG of the CNCs host matrix overlaps with its collective SPR band of the embedded GNPs. Optical studies confirm a distinct blue-shift in both PBG for CNCs matrix and collective SPR band for GNPs. The experimental extinction spectra of CNCG-3g record at incidence angle from 90° to 45° exhibiting single robust coupled SPR-PBG peaks with maxima centered from 556 to 531 nm. In addition, the coupled SPR-PBG optical property shows a linear relationship between the peak wavelength and the value of sin θ for incidence light in the tested spectra range (Figure S8), implying the dominant character of PBG in this optical coupling. When the incidence angle is smaller than θ = 40°, a distinct separation of the

DOI: 10.1021/acsami.5b05645
ACS Appl. Mater. Interfaces 2015, 7, 21797−21806

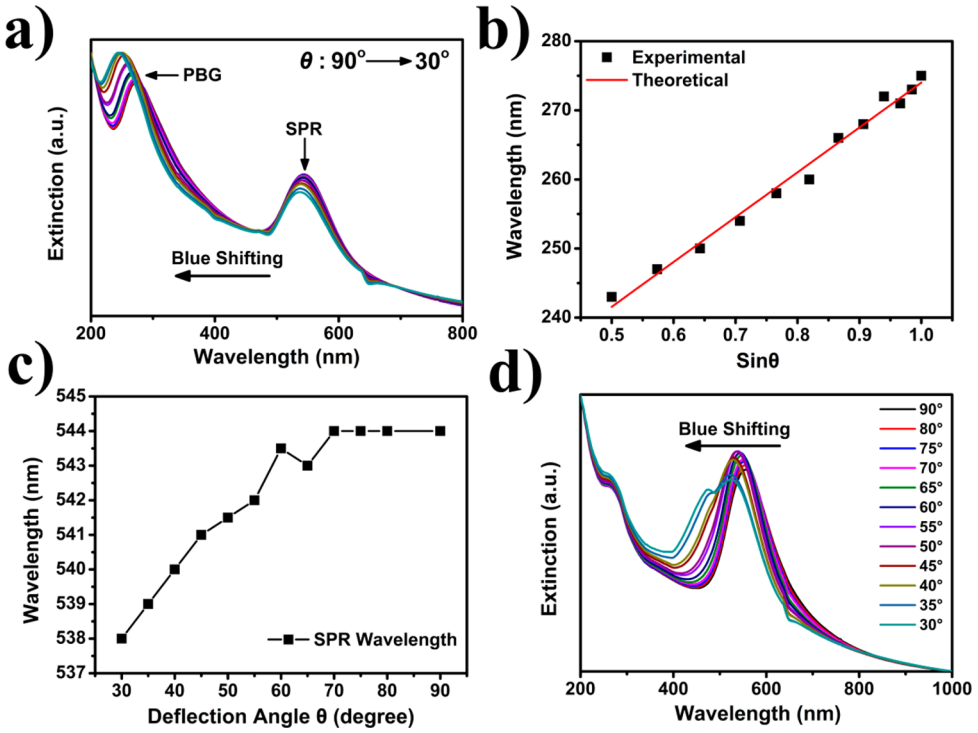

Figure 8. (a) Angle resolved steady-state UV−visible spectra of the sample CNCG-1g, showing a distinct angle-dependent blue shift both in PBG and SPR wavelength peak. (b) Plot of the PBG peak wavelength versus the sine of angle of incidence for CNCG-1g. The data were fitted well with a linear curve. (c) Collective SPR peak wavelength as a function of the incidence angle for CNCG-1g. The peak wavelength blue shifts as the incidence angle decreased from 90° to 30°. (d) Angle resolved UV−visible spectra of the sample CNCG-2g, exhibiting the angle induced separation of the coupled optical property between collective SPR for GNPs and PBG for CNCs host matrix.

coupled SPR-PBG peak is observed. The UV−visible spectra (from 40° to 30°) shows new split doublet phenomena that can be ascribed to the PBG of CNCs matrix (centered from 481 to 470 nm) and the collective SPR of GNPs (centered from 528 to 524 nm), respectively. When the SPR mode of GNPs is coupled with the resonant mode of the chiral nematic CNCs host matrix, the total angle-dependent blue shift value for the collective SPR band is $\Delta\lambda_{SPR}$ = 20 nm. Our experimental observations point to conclude that it is possible to manipulate the separation of the coupling between the collective SPR mode and PBG in CNCs matrix by varying the incidence angle.

The results shown in Figure 8 demonstrate the ability to tune the coupled optical property of SPR-PBG of the CNCG film by altering the incidence angle of the excitation light. And it also reveals that the plasmonic−photonic coupling in the CNCG composites can influence the angle-dependent SPR shifting values. The coupling effect of SPR and PBG has been observed in three-dimensional photonic crystals (opal or inverse opal) with embedded plasmonic metal nanoparticles.[40−44] So far, the electromagnetic properties of GNPs in chiral photonic media have been little investigated, and accurate control over the shift of the SPR peak by varying the incidence angle still remains a major challenge. The optical measurements in previous studies show an angle-tunable PBG of the host photonic crystal, but with an angle-independent plasmonic peak of the embedded nanoparticles. According to Mie's theory, the plasmon resonance for spherical nanoparticles is extremely sensitive to the refractive index of the surrounding medium, but the incidence angle has little effect on the collective SPR.[62] However, on one hand it should be noted that some recent theoretical works indicate when noble nanoparticles are assembled on a planar substrate, they could exhibit nonlinear shifts of the collective SPR wavelength depended on the excitation conditions, such as the distance between the adjacent nanoparticles, the polarization of the incident light and the angle of the incidence excitation electromagnetic wave, etc.[63−65] In the current work, FIB observation in Figure 3d shows that the embedded GNPs are distributed randomly and the distances between neighboring GNPs are too far; therefore, the GNPs are essentially noninteracting with each other and the electromagnetic interactions induced SPR shifting between GNPs should be excluded. It appears that the angle-resolved spectra of the current work do not accord with either the classic Mie's theory or the theoretical predictions. Comparing with previous work,[40−44] we notice that the angle-dependent SPR shifting may associate with the special structure of the chiral nematic ordering of the CNCs host matrix. For further confirmation, we have prepared a nonordered CNCs−GNPs composite with the same GNPs loading as a comparison (Supporting Information). SEM image indicates we have completely destroyed the periodic chiral nematic ordering of the CNCs host matrix (Figure S9). The corresponding angle-resolved spectra show that the SPR peak of the embedded GNPs remains stationary, no angle-dependent SPR shifting occurs at 544 nm (Figure S10). We therefore conclude that the chiral nematic structure of the CNCs host matrix should play an important role in the angle-dependent modulation of SPR shifting. We postulate that this may be due to the filtering effect inside the chiral nematic ordering, in which only left-handed circularly polarized electromagnetic wave can pass through the chiral CNCs matrix and excite the GNPs.[66] Light propagation inside the chiral nematic photonic CNCs matrix is polarized,[67] which is in striking contrast to nonpolarized three-dimensional photonic crystals and randomly packed CNCs nanorods.

DOI: 10.1021/acsami.5b05645
ACS Appl. Mater. Interfaces 2015, 7, 21797−21806

Previous work has pointed out that the SPR peak of GNPs is sensitive to the polarization states of the incident beam and its incidence angle,[65] thus, this specific angle-dependent collective SPR wavelength shifting may arise from the electromagnetic coupling between the embedded GNPs and the circularly polarized light inside the chiral nematic CNCs matrix. At the moment, it is not clear what is the actual mechanism for the angle-dependent SPR shifting in the CNCG films. However, we have found this shifting phenomenon even exists in the transient spectra regime. The ultrafast transient optical response of CNCG films can be strongly tailored by varying the angle of incidence of the probe beam, resulting in a distinct blue shift of the negative transient peak (Figure S11). These results imply that the angle-dependent SPR shifting in the chiral nematic photonic crystal may be a general property, and further investigations (such as finite-difference time-domain calculations) await to be conducted to reveal the governing mechanism more clearly.

CONCLUSION

In summary, we have developed a family of free-standing chiral plasmonic films by embedding GNPs into a chiral nematic CNCs host matrix. The GNPs stay apart and distribute randomly in the chiral nematic organization of CNCs nanorods. These host−guest composite films not only exhibit tunable and switchable plasmonic optical property but also show strong angle-dependent SPR wavelength peak. The current work demonstrates that the noble metal nanoparticle-doped chiral nematic films can be organized by a facile, cost-effective and scalable approach that may be applicable to the development of advanced functional materials such as plasmonic modulators (increase or decrease of the SPR signal intensity) or switches (SPR spectral shift of the stationary/transient optical mode) based on the special angle-sensitive plasmonic property. The current approach may be extended to the assembly of free-standing composite films by including a variety of nanoparticles of different geometry and composition including magnetic, plasmonic or luminescent nanoparticles. In addition, considering the significance of using the collective SPR of metal nanoparticles in sensing, the observed strong plasmonic−photonic coupling and chiral environment of the host substrate may allow for the development of ultrasensitive biosensors based on surface enhanced Raman detection for chiral molecule with high signal-to-noise ratio in real-time measurements,[68] and tuning the SPR wavelength peak by altering the incidence angle of the excitation light in chiral photonic crystal can add an extra degree of freedom and flexibility to open up a new avenue for the design of advanced nonlinear optics materials.[69]

ASSOCIATED CONTENT

Supporting Information

The Supporting Information is available free of charge on the ACS Publications website at DOI: 10.1021/acsami.5b05645.

POM images, UV−visible spectra, CD spectra and plots, as well as charts (PDF).

AUTHOR INFORMATION

Corresponding Author

*Y. Xu. E-mail: yanxu@jlu.edu.cn.

Author Contributions

G.C. synthesized the CNCs−GNPs composite films and carried out the FIB, POM, CD and steady-state UV−visible measurements. H.Y. and G.C. accomplished the ultrafast transient spectra. G.C. designed and led the project. The paper was written through contributions of all authors. All authors have given approval to the final version of the paper.

Notes

The authors declare no competing financial interest.

ACKNOWLEDGMENTS

This work was supported by the National Natural Science Foundation of China (21171067, 21373100), Jilin Provincial Talent Funds (802110000412) and Tang Aoqing Professor Funds of Jilin University (450091105161). The authors thank Professor Xiao-An Zhang for the valuable assistance in POM imaging analysis.

REFERENCES

(1) Yablonovitch, E. Inhibited Spontaneous Emission in Solid-State Physics and Electronics. *Phys. Rev. Lett.* **1987**, *58*, 2059−2062.
(2) John, S. Strong Localization of Photons in Certain Disordered Dielectric Superlattices. *Phys. Rev. Lett.* **1987**, *58*, 2486−2489.
(3) Whitesides, G. M.; Grzybowski, B. Self-Assembly at All Scales. *Science* **2002**, *295*, 2418−2421.
(4) Lodahl, P.; Van Driel, A. F.; Nikolaev, I. S.; Irman, A.; Overgaag, K.; Vanmaekelbergh, D.; Vos, W. L. Controlling the Dynamics of Spontaneous Emission from Quantum Dots by Photonic Crystals. *Nature* **2004**, *430*, 654−657.
(5) Rotello, V. M. Nanoparticles: Building Blocks for Nanotechnology; Springer Science & Business Media: Berlin, 2004.
(6) Zhang, Z.; Zhang, L.; Hedhili, M. N.; Zhang, H.; Wang, P. Plasmonic Gold Nanocrystals Coupled with Photonic Crystal Seamlessly on TiO_2 Nanotube Photoelectrodes for Efficient Visible Light Photoelectrochemical Water Splitting. *Nano Lett.* **2013**, *13*, 14−20.
(7) Lu, Y.; Yu, H.; Chen, S.; Quan, X.; Zhao, H. Integrating Plasmonic Nanoparticles with TiO_2 Photonic Crystal for Enhancement of Visible-Light-Driven Photocatalysis. *Environ. Sci. Technol.* **2012**, *46*, 1724−1730.
(8) Asher, S. A.; Alexeev, V. L.; Goponenko, A. V.; Sharma, A. C.; Lednev, I. K.; Wilcox, C. S.; Finegold, D. N. Photonic Crystal Carbohydrate Sensors: Low Ionic Strength Sugar Sensing. *J. Am. Chem. Soc.* **2003**, *125*, 3322−3329.
(9) Kubo, S.; Gu, Z. Z.; Tryk, D. A.; Ohko, Y.; Sato, O.; Fujishima, A. Metal-Coated Colloidal Crystal Film as Surface-Enhanced Raman Scattering Substrate. *Langmuir* **2002**, *18*, 5043−5046.
(10) Wang, Y.; Li, Q. Light-Driven Chiral Molecular Switches or Motors in Liquid Crystals. *Adv. Mater.* **2012**, *24*, 1926−1945.
(11) Bisoyi, H. K.; Li, Q. Light-Directing Chiral Liquid Crystal Nanostructures: From 1D to 3D. *Acc. Chem. Res.* **2014**, *47*, 3184−3195.
(12) Jiang, X.; Xie, Y.; Lu, J.; Zhu, L.; He, W.; Qian, Y. Simultaneous in Situ Formation of ZnS Nanowires in a Liquid Crystal Template by Υ-Irradiation. *Chem. Mater.* **2001**, *13*, 1213−1218.
(13) Shimoda, Y.; Ozaki, M.; Yoshino, K. Electric Field Tuning of a Stop Band in a Reflection Spectrum of Synthetic Opal Infiltrated with Nematic Liquid Crystal. *Appl. Phys. Lett.* **2001**, *79*, 3627−3629.
(14) Hubbe, M. A.; Rojas, O. J.; Lucia, L. A.; Sain, M. Cellulosic Nanocomposites: A Review. *BioResources* **2008**, *3*, 929−980.
(15) Sacui, I. A.; Nieuwendaal, R. C.; Burnett, D. J.; Stranick, S. J.; Jorfi, M.; Weder, C.; Foster, E. J.; Olsson, R. T.; Gilman, J. W. Comparison of the Properties of Cellulose Nanocrystals and Cellulose Nanofibrils Isolated from Bacteria, Tunicate, and Wood Processed Using Acid, Enzymatic, Mechanical, and Oxidative Methods. *ACS Appl. Mater. Interfaces* **2014**, *6*, 6127−6138.
(16) Habibi, Y.; Lucia, L. A.; Rojas, O. J. Cellulose Nanocrystals: Chemistry, Self-Assembly, and Applications. *Chem. Rev.* **2010**, *110*, 3479−3500.

DOI: 10.1021/acsami.5b05645
ACS Appl. Mater. Interfaces 2015, 7, 21797−21806

(17) Lagerwall, J. P.; Schütz, C.; Salajkova, M.; Noh, J.; Park, J. H.; Scalia, G.; Bergström, L. Cellulose Nanocrystal-Based Materials: From Liquid Crystal Self-Assembly and Glass Formation to Multifunctional Thin Films. *NPG Asia Mater.* **2014**, *6*, e80.
(18) Bondeson, D.; Mathew, A.; Oksman, K. Optimization of the Isolation of Nanocrystals from Microcrystalline Cellulose by Acid Hydrolysis. *Cellulose* **2006**, *13*, 171−180.
(19) Onsager, L. The Effects of Shape on the Interaction of Colloidal Particles. *Ann. N. Y. Acad. Sci.* **1949**, *51*, 627−659.
(20) Beck-Candanedo, S.; Roman, M.; Gray, D. G. Effect of Reaction Conditions on the Properties and Behavior of Wood Cellulose Nanocrystal Suspensions. *Biomacromolecules* **2005**, *6*, 1048−1054.
(21) Vignolini, S.; Rudall, P. J.; Rowland, A. V.; Reed, A.; Moyroud, E.; Faden, R. B.; Baumberg, J. J.; Glover, B. J.; Steiner, U. Pointillist Structural Color in Pollia Fruit. *Proc. Natl. Acad. Sci. U. S. A.* **2012**, *109*, 15712−15715.
(22) Sharma, V.; Crne, M.; Park, J. O.; Srinivasarao, M. Structural Origin of Circularly Polarized Iridescence in Jeweled Beetles. *Science* **2009**, *325*, 449−451.
(23) Bahr, C.; Kitzerow, H. S. *Chirality in Liquid Crystals*; Springer: New York, 2001.
(24) Xue, J.; Song, F.; Yin, X. W.; Wang, X. L.; Wang, Y. Z. Let It Shine: A Transparent and Photoluminescent Foldable Nanocellulose/Quantum Dot Paper. *ACS Appl. Mater. Interfaces* **2015**, *7*, 10076−10079.
(25) Chu, G.; Wang, X.; Chen, T.; Xu, W.; Wang, Y.; Song, H.; Xu, Y. Chiral Electronic Transitions of YVO_4: Eu^{3+} Nanoparticles in Cellulose Based Photonic Materials with Circularly Polarized Excitation. *J. Mater. Chem. C* **2015**, *3*, 3384−3390.
(26) Nguyen, T. D.; Hamad, W. Y.; MacLachlan, M. J. CdS Quantum Dots Encapsulated in Chiral Nematic Mesoporous Silica: New Iridescent and Luminescent Materials. *Adv. Funct. Mater.* **2014**, *24*, 777−783.
(27) Chu, G.; Feng, J.; Wang, Y.; Zhang, X.; Xu, Y.; Zhang, H. Chiral Nematic Mesoporous Films of ZrO_2: Eu^{3+}: New Luminescent Materials. *Dalton Trans.* **2014**, *43*, 15321−15327.
(28) Chu, G.; Xu, W.; Qu, D.; Wang, Y.; Song, H.; Xu, Y. Chiral Nematic Mesoporous Films of Y_2O_3: Eu^{3+} with Tunable Optical Properties and Modulated Photoluminescence. *J. Mater. Chem. C* **2014**, *2*, 9189−9195.
(29) Chu, G.; Wang, X.; Chen, T.; Gao, J.; Gai, F.; Wang, Y.; Xu, Y. Optically Tunable Chiral Plasmonic Guest-Host Cellulose Films Weaved with Long-Range Ordered Silver Nanowires. *ACS Appl. Mater. Interfaces* **2015**, *7*, 11863−11870.
(30) Lukach, A.; Thérien-Aubin, H.; Querejeta-Fernández, A.; Pitch, N.; Chauve, G.; Méthot, M.; Bouchard, J.; Kumacheva, E. Coassembly of Gold Nanoparticles and Cellulose Nanocrystals in Composite Films. *Langmuir* **2015**, *31*, 5033−5041.
(31) Querejeta-Fernández, A.; Chauve, G. g.; Methot, M.; Bouchard, J.; Kumacheva, E. Chiral Plasmonic Films Formed by Gold Nanorods and Cellulose Nanocrystals. *J. Am. Chem. Soc.* **2014**, *136*, 4788−4793.
(32) Liu, Q.; Campbell, M. G.; Evans, J. S.; Smalyukh, I. I. Orientationally Ordered Colloidal Co-Dispersions of Gold Nanorods and Cellulose Nanocrystals. *Adv. Mater.* **2014**, *26*, 7178−7184.
(33) Schlesinger, M.; Giese, M.; Blusch, L. K.; Hamad, W. Y.; MacLachlan, M. J. Chiral Nematic Cellulose-Gold Nanoparticle Composites from Mesoporous Photonic Cellulose. *Chem. Commun.* **2015**, *51*, 530−533.
(34) Schlesinger, M.; Hamad, W. Y.; MacLachlan, M. J. Optically Tunable Chiral Nematic Mesoporous Cellulose Films. *Soft Matter* **2015**, *11*, 4686−4694.
(35) Thérien-Aubin, H.; Lukach, A.; Pitch, N.; Kumacheva, E. Coassembly of Nanorods and Nanospheres in Suspensions and in Stratified Films. *Angew. Chem., Int. Ed.* **2015**, *127*, 5710−5714.
(36) Thérien-Aubin, H.; Lukach, A.; Pitch, N.; Kumacheva, E. Structure and Properties of Composite Films Formed by Cellulose Nanocrystals and Charged Latex Nanoparticles. *Nanoscale* **2015**, *7*, 6612−6618.
(37) Dong, S.; Roman, M. Fluorescently Labeled Cellulose Nanocrystals for Bioimaging Applications. *J. Am. Chem. Soc.* **2007**, *129*, 13810−13811.
(38) Shopsowitz, K. E.; Qi, H.; Hamad, W. Y.; MacLachlan, M. J. Free-Standing Mesoporous Silica Films with Tunable Chiral Nematic Structures. *Nature* **2010**, *468*, 422−425.
(39) Shopsowitz, K. E.; Kelly, J. A.; Hamad, W. Y.; MacLachlan, M. J. Biopolymer Templated Glass with a Twist: Controlling the Chirality, Porosity, and Photonic Properties of Silica with Cellulose Nanocrystals. *Adv. Funct. Mater.* **2014**, *24*, 327−338.
(40) Wang, D.; Salgueiriño-Maceira, V.; Liz-Marzán, L. M.; Caruso, F. Gold-Silica Inverse Opals by Colloidal Crystal Templating. *Adv. Mater.* **2002**, *14*, 908−912.
(41) Vasquez, Y.; Kolle, M.; Mishchenko, L.; Hatton, B. D.; Aizenberg, J. Three-Phase Co-Assembly: In Situ Incorporation of Nanoparticles into Tunable, Highly Ordered, Porous Silica Films. *ACS Photonics* **2014**, *1*, 53−60.
(42) Tan, Y.; Qian, W.; Ding, S.; Wang, Y. Gold-Nanoparticle-Infiltrated Polystyrene Inverse Opals: A Three-Dimensional Platform for Generating Combined Optical Properties. *Chem. Mater.* **2006**, *18*, 3385−3389.
(43) Ding, S.; Qian, W.; Tan, Y.; Wang, Y. In-Situ Incorporation of Gold Nanoparticles of Desired Sizes into Three-Dimensional Macroporous Matrixes. *Langmuir* **2006**, *22*, 7105−7108.
(44) Wang, D.; Li, J.; Chan, C.; Salgueiriño-Maceira, V.; Liz-Marzán, L. M.; Romanov, S.; Caruso, F. Optical Properties of Nanoparticle-Based Metallodielectric Inverse Opals. *Small* **2005**, *1*, 122−130.
(45) Blokhin, A.; Gelin, M.; Buganov, O.; Dubovskii, V.; Tikhomirov, S.; Tolstorozhev, G. Femtosecond Dynamics of Optically Induced Anisotropy of Complex Molecules in the Gas Phase. *J. Appl. Spectrosc.* **2003**, *70*, 70−78.
(46) Liu, J.; Lu, Y. Preparation of Aptamer-Linked Gold Nanoparticle Purple Aggregates for Colorimetric Sensing of Analytes. *Nat. Protoc.* **2006**, *1*, 246−252.
(47) Bardet, R.; Belgacem, N.; Bras, J. Flexibility and Color Monitoring of Cellulose Nanocrystal Iridescent Solid Films Using Anionic or Neutral Polymers. *ACS Appl. Mater. Interfaces* **2015**, *7*, 4010−4018.
(48) Pan, J.; Hamad, W.; Straus, S. K. Parameters Affecting the Chiral Nematic Phase of Nanocrystalline Cellulose Films. *Macromolecules* **2010**, *43*, 3851−3858.
(49) Jenkins, J. A.; Zhou, Y.; Thota, S.; Tian, X.; Zhao, X.; Zou, S.; Zhao, J. Blue-Shifted Narrow Localized Surface Plasmon Resonance from Dipole Coupling in Gold Nanoparticle Random Arrays. *J. Phys. Chem. C* **2014**, *118*, 26276−26283.
(50) Wang, X.; Gogol, P.; Cambril, E.; Palpant, B. Near-and Far-Field Effects on the Plasmon Coupling in Gold Nanoparticle Arrays. *J. Phys. Chem. C* **2012**, *116*, 24741−24747.
(51) Beck, S.; Bouchard, J.; Berry, R. Controlling the Reflection Wavelength of Iridescent Solid Films of Nanocrystalline Cellulose. *Biomacromolecules* **2011**, *12*, 167−172.
(52) Dong, X. M.; Gray, D. G. Effect of Counterions on Ordered Phase Formation in Suspensions of Charged Rodlike Cellulose Crystallites. *Langmuir* **1997**, *13*, 2404−2409.
(53) Ozbay, E. Plasmonics: Merging Photonics and Electronics at Nanoscale Dimensions. *Science* **2006**, *311*, 189−193.
(54) Wang, X.; Palpant, B. Large and Ultrafast Optical Response of a One-Dimensional Plasmonic-Photonic Cavity. *Plasmonics* **2013**, *8*, 1647−1653.
(55) Wang, X.; Morea, R.; Gonzalo, J.; Palpant, B. Coupling Localized Plasmonic and Photonic Modes Tailors and Boosts Ultrafast Light Modulation by Gold Nanoparticles. *Nano Lett.* **2015**, *15*, 2633−2639.
(56) Yeom, B.; Zhang, H.; Zhang, H.; Park, J. I.; Kim, K.; Govorov, A. O.; Kotov, N. A. Chiral Plasmonic Nanostructures on Achiral Nanopillars. *Nano Lett.* **2013**, *13*, 5277−5283.
(57) Fan, Z.; Govorov, A. O. Plasmonic Circular Dichroism of Chiral Metal Nanoparticle Assemblies. *Nano Lett.* **2010**, *10*, 2580−2587.

DOI: 10.1021/acsami.5b05645
ACS Appl. Mater. Interfaces 2015, 7, 21797−21806

(58) De Vries, H. Rotatory Power and Other Optical Properties of Certain Liquid Crystals. *Acta Crystallogr.* **1951**, *4*, 219−226.
(59) Giese, M.; Blusch, L. K.; Khan, M. K.; Hamad, W. Y.; MacLachlan, M. J. Responsive Mesoporous Photonic Cellulose Films by Supramolecular Cotemplating. *Angew. Chem., Int. Ed.* **2014**, *53*, 8880−8884.
(60) Wang, F.; Zhu, Z.; Meng, Z.; Xue, F.; Wang, Q.; Xue, M.; Lu, W.; Chen, W.; Qi, F.; Yan, Z. Cellulose Photonic Crystal Film Sensor for Alcohols. *Sens. Actuators, B* **2015**, *220*, 222−226.
(61) Zhang, Y. P.; Chodavarapu, V. P.; Kirk, A. G.; Andrews, M. P. Structured Color Humidity Indicator from Reversible Pitch Tuning in Self-Assembled Nanocrystalline Cellulose Films. *Sens. Actuators, B* **2013**, *176*, 692−697.
(62) Link, S.; El-Sayed, M. A. Size and Temperature Dependence of the Plasmon Absorption of Colloidal Gold Nanoparticles. *J. Phys. Chem. B* **1999**, *103*, 4212−4217.
(63) Pinchuk, A. O. Angle Dependent Collective Surface Plasmon Resonance in an Array of Silver Nanoparticles. *J. Phys. Chem. A* **2009**, *113*, 4430−4436.
(64) King, N. S.; Li, Y.; Ayala-Orozco, C.; Brannan, T.; Nordlander, P.; Halas, N. J. Angle-and Spectral-Dependent Light Scattering from Plasmonic Nanocups. *ACS Nano* **2011**, *5*, 7254−7262.
(65) Lodewijks, K.; Van Roy, W.; Borghs, G.; Lagae, L.; Van Dorpe, P. Boosting the Figure-of-Merit of LSPR-Based Refractive Index Sensing by Phase-Sensitive Measurements. *Nano Lett.* **2012**, *12*, 1655−1659.
(66) Prost, J. *The Physics of Liquid Crystals*; Oxford University Press: Oxford, U. K., 1995.
(67) Woon, K. L.; O'Neill, M.; Richards, G. J.; Aldred, M. P.; Kelly, S. M. Stokes Parameter Studies of Spontaneous Emission from Chiral Nematic Liquid Crystals as a One-Dimensional Photonic Stopband Crystal: Experiment and Theory. *Phys. Rev. E* **2005**, *71*, 041706.
(68) Huang, Y.; Fang, Y.; Zhang, Z.; Zhu, L.; Sun, M. Nanowire-Supported Plasmonic Waveguide for Remote Excitation of Surface-Enhanced Raman Scattering. *Light: Sci. Appl.* **2014**, *3*, e199.
(69) Gao, H.; Yang, J. C.; Lin, J. Y.; Stuparu, A. D.; Lee, M. H.; Mrksich, M.; Odom, T. W. Using the Angle-Dependent Resonances of Molded Plasmonic Crystals to Improve the Sensitivities of Biosensors. *Nano Lett.* **2010**, *10*, 2549−2554.

DOI: 10.1021/acsami.5b05645
ACS Appl. Mater. Interfaces 2015, 7, 21797−21806